International Journal of Applied Mechanics
Vol. 13, No. 4 (2021) 2150059 (17 pages)

DOI: 10.1142/S1758825121500599

Hybrid Simulation of Turbulent Natural Convection in an Enclosure with Thermally-Conductive Walls

Alexander Nee*

Research and Educational Center of I.N. Butakov
National Research Tomsk Polytechnic University, Tomsk, Russia
nee_alexander@mail.ru

Ali J. Chamkha

Faculty of Engineering, Kuwait College of Science and Technology
Doha District, Kuwait
Center of Excellence in Desalination Technology
King Abdulaziz University, P.O. Box 80200
Jeddah 21589, Saudi Arabia
a.chamkha@kcst.edu.kw

Received 15 April 2021
Accepted 3 July 2021
Published 16 September 2021

This paper analyzes the interaction of high Rayleigh number flow with conjugate heat transfer. The two-relaxation time lattice Boltzmann is used as a turbulent buoyancy-driven flow solver whereas the implicit finite difference technique is applied as a heat transfer solver. An in-house numerical code is developed and successfully validated on typical CFD problems. The impact of the Biot number, heat diffusivity ratio and the Rayleigh number on turbulent fluid flow and heat transfer patterns is studied. It is revealed that the thermally-conductive walls of finite thickness reduce the heat transfer rate. The temperature of the cooled wall slightly depends on the value of the buoyancy force. The heat diffusivity ratio has a significant effect on thermal and flow behavior. The Biot number significantly affects the mean Nusselt number at the right solid–fluid interface whereas the mean Nusselt number at the left interface is almost insensible to the Biot number variation.

Keywords: Hybrid LBM; turbulent natural convection; FDM; conjugate heat transfer.

Nomenclature

a : Thermal diffusivity, m^2/s
Bi : Kirpichev number $= (\alpha \cdot L)/\lambda_s$;
Ki : Kirpichev number $= (q \cdot L)/(\lambda_s \cdot (T_h - T_c))$
l : Thickness of the walls, m;

*Corresponding author.

L : Length of the cavity, m;
Pr : Prandtl number $= \nu/a$;
q : Heat flux, W/m^2
Ra : Rayleigh number $= (g \cdot \beta \cdot (T_h - T_c) \cdot L^3)/(\nu \cdot a)$;
t : Time, s;
t_0 : Time scale, s;
Δt : Time step in lattice Boltzmann equation;
u, v : Velocities components, m/s;
U, V : Dimensionless analogues of u, v;
V_{nc} : Velocity scale, m/s;
w_k : Weighting factor;

Greek symbols

α : Heat transfer coefficient, W/(m$^2 \cdot$ K);
λ : Heat conductivity coefficient, W/(m $\cdot$ K);
τ : Dimensionless time;
Θ : Dimensionless temperature;

Subsripts

c : cold wall.
a : ambient;
f : fluid region;
h : hot wall;
s : solid region.

1. Introduction

Heat transfer by turbulent natural convection coupled with heat conduction in the solid walls is extensively studied due to engineering applications such as HVAC systems, solar collectors, fuel cells cooling, etc. In spite of the significant development of numerical tools, an accurate patterns prediction of developed turbulent buoyancy driven flows is still a big challenge.

In order to study turbulent flow and thermal behavior under the conjugate formulation, Ben Yedder and Bilgen [2008] proposed to use the Reynolds-averaged Navier–Stokes (RANS) equations. To define turbulent viscosity, the standard k–ε model was applied. It should be stressed that turbulent buoyancy driven flows in enclosures with heat-conducting walls of finite thickness is of great interest in terms of the building thermophysics applications. Ben-Nakhi and Mahmoud [2008] studied turbulent natural convection inside a building attic applying winter day boundary conditions. Examination was performed by means of the RANS approach with the low-Reynolds-number SST k–ω turbulence model. It was found that the heat flux through the external wall bypassed the heat insulation due to thermal bridging. Xaman *et al.* [2008] considered turbulent natural convection combined with surface thermal radiation in a square cavity with a glass heat-conducting wall. After that,

Xaman *et al.* [2009] studied how a selective coating at the inner side of the glass wall affected the solar radiation transmission. Later, the effect of the glass wall size was examined under the same conditions [Olazo-Gomez *et al.*, 2020]. It should be noted that the above studies were conducted in terms of the RANS standard k–ε model. Mikhailenko *et al.* [2020] examined conjugate heat transfer and turbulent fluid flow inside a room with a so-called "warm floor" system. Surface thermal radiation was taken into account and the RANS method with standard k–ε model was applied. It was found that natural convective mechanism of heat transfer was weakened with an increase in the surface emissivity.

A significant contribution in the field of conjugate heat transfer is made by Sheremet *et al.* Kuznetsov and Sheremet [2010] analyzed the two-dimensional turbulent buoyancy-driven flow in a domain bounded by walls of finite thickness with a local convective heater. The governing equations were formulated in terms of the stream function–vorticity dimensionless variables. Standard model of kinetic energy and its dissipation rate within RANS approach was used to study turbulent flow and thermal behavior. Three-dimensional conjugate natural convection was considered in [Sheremet and Miroshnichenko, 2015]. Reynolds averaged pressure–velocity formulation coupled with the standard k–ε model was applied to analyze 3D flow patterns. Later, the authors have studied combined conjugate natural convection with radiation. Along with that, Sheremet *et al.* [2016, 2018] proposed to perform specific coordinate transformation in order to improve the accuracy of the standard k–ε model.

Sergent *et al.* [2013a,b] and Xin *et al.* [2013] performed a series of studies in order to understand the discrepancy between numerical and experimental data obtained for the cavity heated from the side. The authors conducted a direct numerical simulation (DNS) and a large eddy simulation (LES) with the Rayleigh number of 1.5×10^9. It was found that the error in horizontal velocity component and temperature near the boundaries was reduced when taking into account heat conduction in the solid walls.

Whereas the above studies analyzed heat transfer and turbulent fluid flow regularities in Cartesian coordinates, Sharma *et al.* [2008] considered turbulent natural convection of a liquid metal in a cylindrical enclosure. The governing equations were formulated within the Reynolds-averaged Navier–Stokes approach. The standard k–ε model was applied to determine the turbulent viscosity.

To summarize the above, a reasonable conclusion is made that interaction of turbulent natural convection and heat conduction in the finite thickness walls is predominantly studied by means of the semi-empirical RANS models. Moreover, an accurate DNS under conjugate heat transfer conditions was performed for low turbulent buoyancy driven flows with the $Ra = 1.5 \times 10^9$. In order to study the high turbulent flows by means of the conventional DNS, computational grid should be significantly refined. As a result, processing times are drastically increased and become unacceptable. On the other hand, alternative CFD tool named lattice Boltzmann

(LBM) [Rahimi *et al.*, 2019] is extensively developed. LBM allows to study turbulent natural convection [Dixit and Babu, 2006; Sharma and Straka, 2018] with the Rayleigh number up to 10^{10} with an accuracy much superior to the RANS approach. The great efforts are done within the development of the thermal LBM model called passive scalar or double distribution function approach [Rahimi *et al.*, 2018]. Along with that, a little attention is paid to hybrid formulation [Obrecht *et al.*, 2013; Bettaibi *et al.*, 2016]. Separate solution of lattice Boltzmann equation and advection/diffusion equation by finite difference or control volume techniques provides higher numerical stability as was reported in [Lallemand and Lou, 2003].

To the best of our knowledge, there is a gap in the field of DNS of turbulent natural convection combined with conjugate heat transfer. It should be also stressed that numerical implementation of two-parametric RANS and advanced LBM models is still a big challenge for many researchers. Hence, the aim of this study is to build a simple model to study heat transfer and fluid flow patterns of conjugate turbulent natural convection in terms of the hybrid lattice Boltzmann formulation.

2. Problem Formulation

2.1. *Physical model*

Heat transfer and fluid flow are studied in terms of the square fluid-filled cavity with heat-conducting finite thickness walls. It is assumed that the solution domain (Fig. 1) was heated from the left side by constant heat flux. Heat losses through the right wall to the environment are taken into account by specifying the constant heat transfer coefficient and ambient temperature. The top and bottom walls are heat-insulated. The conjugate boundary conditions are set at the solid-fluid interfaces for the energy equation. The no-slip condition is set for the velocity at the solid walls.

When formulating the physical model, the following assumptions are made:

- Physical properties of solid walls and fluid are temperature-independent.

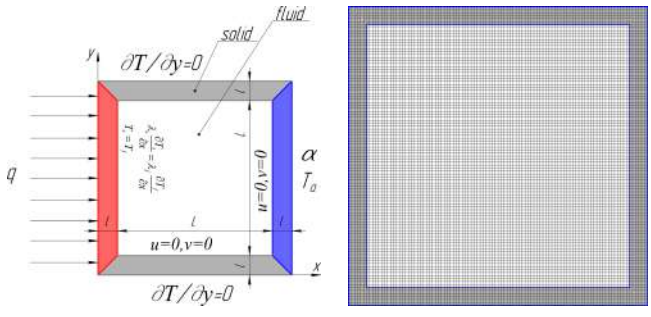

(a) (b)

Fig. 1. Solution domain (a) and computational mesh (b).

- Surface emissivity is equal to zero.
- Fluid is a radiatively non-participating medium.
- Low Mach number viscous incompressible flow is analyzed.
- Fluid satisfies the Boussinesq approximation.
- Viscous energy dissipation term in the energy equation is neglected. The numerical scheme viscosity imitates the physical viscosity under the pseudo-DNS technique used in the present study.
- Turbulence is homogeneous and isotropic.

2.2. *Fluid dynamics model*

When taking into account the assumptions formulated above, fluid dynamics can be described by the following mesoscopic Boltzmann equation:

$$\frac{\partial f}{\partial t} + u \cdot \nabla f = \Omega. \tag{1}$$

The two-relaxation time (TRT) approximation [Ginzburg *et al.*, 2008] is a kind of compromise between BGK and MRT models. On the one hand, implementation of the TRT is as simple as the BGK. On the other hand, the accuracy and stability properties are close to the MRT. The TRT scheme operates with two relaxation rates. The first relaxation rate is related to the shear viscosity, while the other one is a tune coefficient derived through the so-called "magic" parameter Λ. When implementing the TRT approximation and the D2Q9 scheme, the discretized lattice Boltzmann equation is as follows:

$$\begin{aligned} &f_k(\vec{x} + \vec{c}_k \cdot \Delta t,\ t + \Delta t) \\ &\quad = f_k(\vec{x},\ t) - \Delta t \cdot \omega_s \cdot (f_k^s - f_k^{\mathrm{seq}}) - \Delta t \cdot \omega_a \cdot (f_k^a - f_k^{\mathrm{aeq}}) + \Delta t \cdot F, \end{aligned} \tag{2}$$

where f is particle distribution function; $f_k^s = 0.5 \cdot (f_k + f_{-k})$ and $f_k^a = 0.5 \cdot (f_k - f_{-k})$ are symmetrical and asymmetrical parts of distribution function, respectively; $f^{\mathrm{eq}} = w_k \cdot \rho \cdot [1 + \frac{c_k \cdot u}{c_s^2} + \frac{(c_k \cdot u)^2}{2 \cdot c_s^4} - \frac{u^2}{2 \cdot c_s^2}]$ is equilibrium distribution function; $f_k^{\mathrm{seq}} = 0.5 \cdot (f_k^{\mathrm{eq}} + f_{-k}^{\mathrm{eq}})a$ and $f_k^{\mathrm{aeq}} = 0.5 \cdot (f_k^{\mathrm{eq}} - f_{-k}^{\mathrm{eq}})$ are symmetrical and asymmetrical parts of f^{eq}, correspondingly; $w_1 = 4/9$, $w_{2..5} = 1/9$, $w_{6..9} = 1/36$ are weights for D2Q9 model; c_k is speed of particles; c_s is lattice speed of sound; ρ is density; Δt is lattice time step. The subscript "–k" denotes the movement opposite to k (see Fig. 2).

To recover the macroscopic density and velocity, the following relations are used:

$$\rho = \sum_{k=1}^{9} f_k, \tag{3}$$

$$u = \frac{1}{\rho} \cdot \sum_{k=1}^{9} c_k \cdot f_k. \tag{4}$$

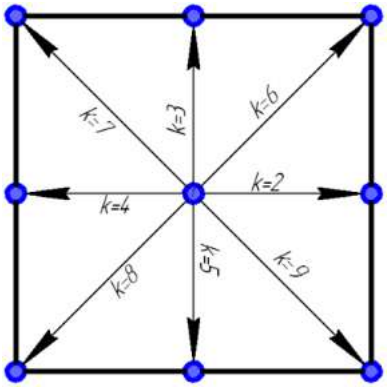

Fig. 2. D2Q9 scheme.

The symmetrical relaxation rate is computed using the kinematic viscosity as

$$\omega_s = \frac{1}{3 \cdot \nu + 0.5}. \tag{5}$$

The symmetrical and asymmetrical relaxation rates are related by so-called "magic" parameter. In order to maintain numerical stability with high Rayleigh numbers, Λ was set to 1/4 as recommended in [Ginzburg *et al.*, 2008].

$$\Lambda = \left(\frac{1}{\omega_s} - 0.5\right) \cdot \left(\frac{1}{\omega_a} - 0.5\right) = \frac{1}{4}. \tag{6}$$

The force term describing buoyancy effects in Eq. (1) is expressed as

$$F = 3 \cdot \rho \cdot w_k \cdot c_y \cdot g \cdot \beta \cdot T, \tag{7}$$

where g is acceleration due to gravity; β is coefficient of volumetric thermal expansion, T is temperature. To model the no-slip condition at the solid walls, a simple bounce back condition was implemented for the distribution function. It was assumed that the distribution function was equal to the equilibrium distribution function at the initial moment of time while the density was set to unity.

2.3. *Heat transfer model*

In this study, thermal behavior is described in terms of the macroscopic energy equation for fluid and the heat conduction equation for the solid area.

Fluid region:

$$\frac{\partial \Theta_f}{\partial \tau} + U\frac{\partial \Theta_f}{\partial X} + V\frac{\partial \Theta_f}{\partial Y} = \frac{1}{\sqrt{Ra \cdot Pr}}\left(\frac{\partial^2 \Theta_f}{\partial X^2} + \frac{\partial^2 \Theta_f}{\partial Y^2}\right). \tag{8}$$

Solid region:

$$\frac{\partial \Theta_s}{\partial \tau} = \frac{a_{s,f}}{\sqrt{Ra \cdot Pr}}\left(\frac{\partial^2 \Theta_s}{\partial X^2} + \frac{\partial^2 \Theta_s}{\partial Y^2}\right). \tag{9}$$

where subscripts f and s represent fluid and solid regions, respectively.

The initial and boundary conditions for energy and heat conduction equations are as follows:

$$\Theta = U = V = 0, \tag{10}$$

at the external boundary of the left wall:

$$\frac{\partial \Theta}{\partial X} = Ki, \tag{11}$$

at the external boundary of the right wall:

$$\frac{\partial \Theta}{\partial X} = Bi \cdot (\Theta - \Theta_a), \tag{12}$$

at the external boundary of the bottom and top walls:

$$\frac{\partial \Theta}{\partial Y} = 0, \tag{13}$$

at the solid-fluid interfaces:

$$\begin{vmatrix} \dfrac{\partial \Theta_s}{\partial n} = \lambda_{f,s} \dfrac{\partial \Theta_f}{\partial n} \\ \Theta_s = \Theta_f. \end{vmatrix}, \tag{14}$$

The mean Nusselt numbers at the vertical solid–fluid interfaces are as follows:

$$\begin{aligned} Nu_L &= \int_l^{l+L} \left.\frac{\partial \Theta}{\partial X}\right|_{X=l} dY, \\ Nu_R &= \int_l^{l+L} \left.\frac{\partial \Theta}{\partial X}\right|_{X=l+L} dY. \end{aligned} \tag{15}$$

To perform a nondimensionalization of Eqs. (9)–(15), the following relations are utilized:

$$X = \frac{x}{L}; \quad Y = \frac{y}{L}; \qquad U = \frac{u}{V_{\text{nc}}}; \quad V = \frac{v}{V_{\text{nc}}}; \quad M = \frac{l}{L};$$

$$V_{\text{nc}} = \sqrt{g \cdot \beta \cdot (T_h - T_c) \cdot L}; \quad \Theta = \frac{T - T_c}{T_h - T_c}; \quad a_{f,s} = \frac{a_f}{a_s}; \quad \lambda_{f,s} = \frac{\lambda_f}{\lambda_s}.$$

To solve the thermal boundary value problem, the finite difference technique is implemented. The second-order partial differential equations are discretized by means of the two layer implicit scheme. The description of numerical implementation of this scheme can be found in the previous works [Kuznetsov *et al.*, 2018; Nee, 2020].

2.4. *Validation*

The solution algorithm used in this study is carefully validated against benchmark numerical data of other researches. The work of Ben Yedder and Bilgen [1997] is

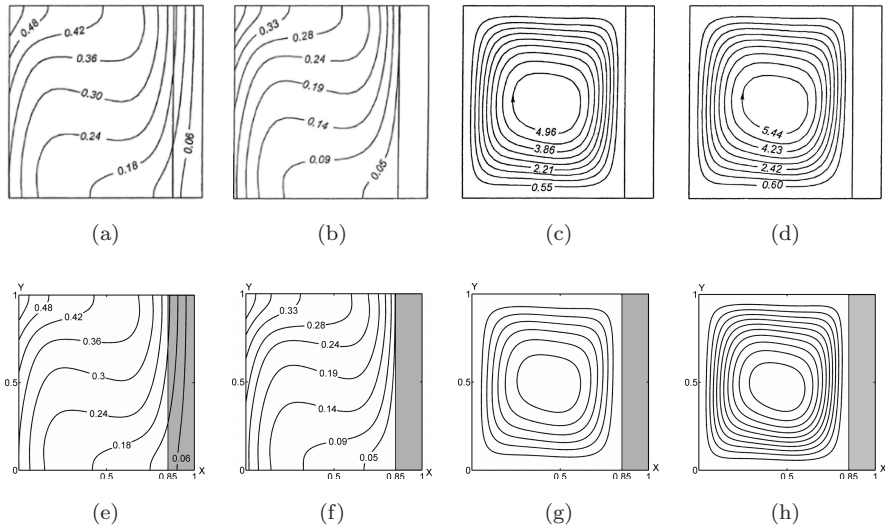

Fig. 3. Steady-state isotherms when $Ra = 10^5$ and $M = 0.15$: (a), (b) Ben Yedder and Bilgen [1997]; (c), (d) this study.

used to assess the fidelity of conjugate heat transfer description. Figure 3 shows temperature contours and streamlines with variation of the heat conductivity ratio $k_r = \frac{\lambda_s}{\lambda_f}$.

In order to check the accuracy of the proposed turbulent natural convection solver, a buoyancy-driven flow in an air-filled differentially heated cavity is analyzed. Validation is performed in terms of the mean Nusselt number at the hot wall in a range of the Rayleigh number considered in the present work. Figure 4 shows the results of the comparative study.

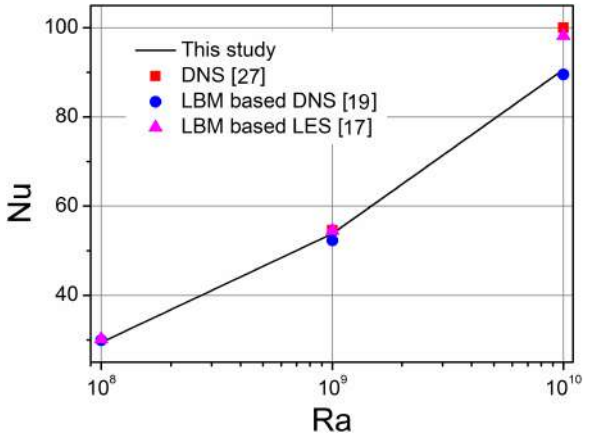

Fig. 4. Variation of the mean Nusselt number with the Rayleigh number.

When analyzing the data presented in Fig. 3, it is found that both conjugate heat transfer and fluid flow characteristics perfectly match with the data of Ben Yedder and Bilgen [1997]. On the other hand, heat transfer rate results (Fig. 4) well correlated with the $Ra \leq 10^9$. When $Ra = 10^{10}$, the mean Nusselt number obtained with hybrid lattice Boltzmann had the same value as in the case of LBM-based DNS Wang *et al.* [2017]. An insignificant error for turbulent flow in an amount of around 8% is revealed when comparing with conventional DNS [Xin and Le Quéré, 1994] and LBM-based LES Zhuo and Zhong [2013] methods. To sum up, a satisfactory agreement with the benchmark data of other researchers is observed. Hence, the proposed hybrid approach is successfully validated.

2.5. *Grid analysis*

A mesh refinement test was performed in order to reach the grid-independent results. Figure 5 presents variation of temperature and vertical velocity component with a number of nodes in the characteristic section of the solution domain.

It must be stressed that a perfect match is hardly achievable in the case of turbulent flow. However, when analyzing the local heat transfer and fluid flow characteristics presented in Fig. 5, quasi grid-independent results are observed between the grid sizes of 721^2 and 841^2. Along with that, the error in the mean Nusselt numbers (Table 1) does not exceed 3 % with a number of 841^2 nodes.

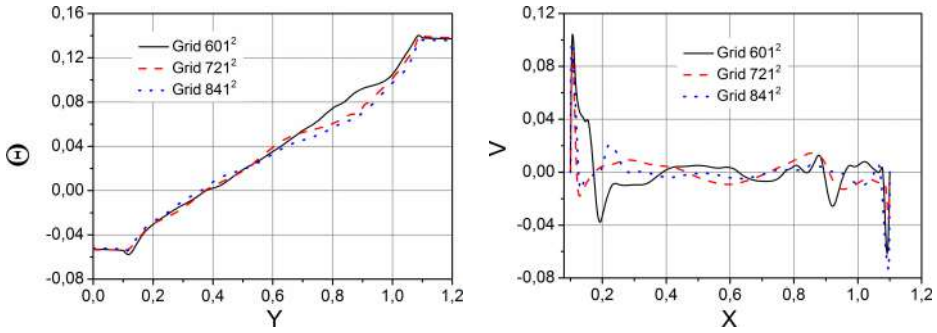

(a) (b)

Fig. 5. Temperature (a) and velocity (b) profiles when $Ra = 10^{10}$, $Pr = 0.71$, $a_{f,s} = 96.79$, $\lambda_{f,s} = 0.074$, $M = 0.1$ in the sections of: a – $X = 0.6$; b – $Y = 0.6$.

Table 1. Variation of mean Nusselt numbers and CPU times for 100000 iterations with the grid size when $Ra = 10^{10}$, $Pr = 0.71$, $a_{f,s} = 96.79$, $\lambda_{f,s} = 0.074$, $M = 0.1$.

Grid	601^2	721^2	841^2	961^2
Nu_L	13.6	14.02	14.23	14.17
Nu_R	9.04	9.68	9.37	9.1
CPU time for Core i3-8100, hours	9.44	14.43	21	27.91

Thus, numerical simulation was conducted on a uniform mesh with a number of 841^2 nodes.

3. Results and Discussion

Interaction of turbulent buoyancy-driven flow with heat conduction in the finite thickness solid walls is examined for the case of square cavity filled with a transparent fluid. When analyzing conjugate heat transfer and turbulent fluid flow characteristics, the Raleigh number is varied from 10^8 to 10^{10}. Variation ranges of the heat diffusivity ratio, Biot number and the heat conductivity ratio are $1.67 \leq a_{f,s} \leq 96.79$, $10 \leq Bi \leq 23$ and $5.6 \times 10^{-4} \leq \lambda_{f,s} \leq 0.260$, respectively. The following parameters such as the Prandtl number $Pr = 0.71$, Kirpichev number $Ki = 1$, dimensionless walls thickness $M = 0.1$ and the ambient temperature $\Theta_a = -0.2$ are constant. All illustrations are given under statistically steady-state conditions. To ensure that this state is reached, at least 500,000 iterations were performed.

3.1. *The effect of Ra*

The thermal and flow behavior is presented in Fig. 6 when varying the Rayleigh number.

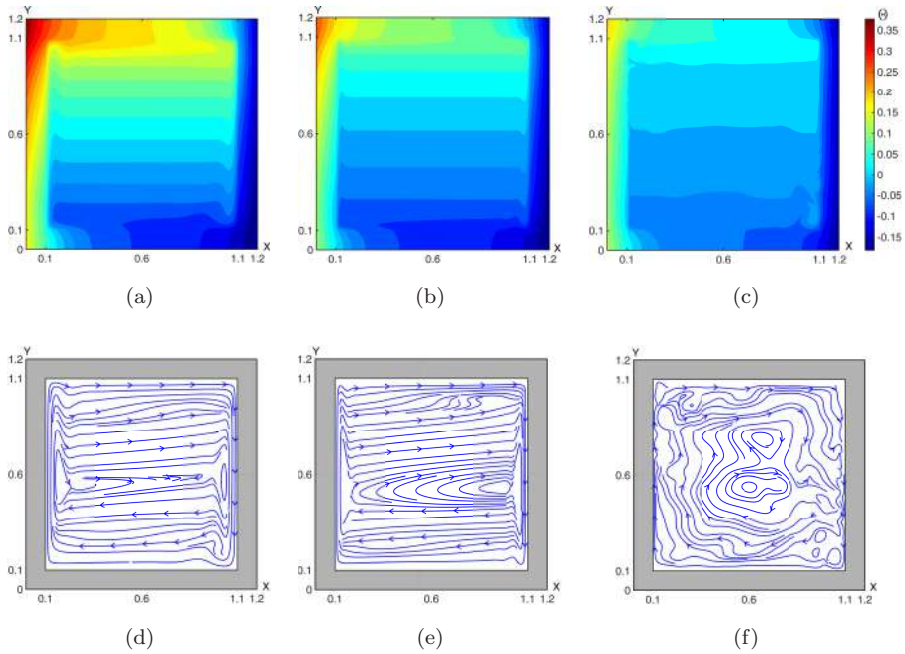

Fig. 6. Temperature fields (a)–(c) and streamslices (d)–(f) when $a_{f,s} = 89.82$, $\lambda_{f,s} = 0.26$ and $Bi = 23$: (a, d) $Ra = 10^8$; (b, e) $Ra = 10^9$; (c, f) $Ra = 10^{10}$.

When performing a general observation, it is found that the side heating and cooling of the analysis domain with constant rate are resulted in the inside thermal stratification. The hottest part of the solution domain is noticed at the top left corner since an up-ward flow of warm air is formed due to natural convective mechanism of heat transfer. It is interesting to note that fluid flow still remains non-oscillatory when the $Ra = 10^9$. Along with that, transition from laminar to turbulent flow behavior is observed with the $Ra \geq 2 \times 10^8$ in the case of the square cavity with perfectly heat-conducting infinitely thin walls. Hence, heat-conducting finite thickness walls weaken the heat transfer rate due to energy accumulation by the solid walls. When increasing the Rayleigh number, the temperature of the heated left wall is reduced since the total thermal resistance is decreased. Monocellular uniform flow is observed with the $Ra = 10^8$. Two secondary vortices are formed near the isothermal walls. It is found that the flow pattern is slightly altered with an increment in the Rayleigh number to $Ra = 10^9$. On the contrary, the temperature of the fluid filling the cavity is reduced. Probably, the heat losses rate is enhanced with an increase in the buoyancy force. A further increase of the Rayleigh number to 10^{10} leads to a drastic change in the flow behavior. The inside flow structure becomes irregular and many small eddies are created. Obviously, these factors contribute to a better mixing of the fluid. Hence, uniform thermal field is formed inside the cavity. Figure 7 represents the temperature and velocity distributions.

When analyzing the data, it is clearly seen that the same trend of temperature is formed under the studied conditions. On the other hand, the velocity curve is drastically changed when the Rayleigh number is equal to 10^{10}. It is revealed that the temperature of the right wall slightly depends on the value of the buoyancy force. On the contrary, the temperature of the bottom/top heat insulated wall is increased/decreased with an increment in the Rayleigh number. A low value of the heat-conductivity coefficient of the enclosure contributes to a formation of the temperature gradient inside the left-heated and right-cooled solid walls. However, there is no temperature gradient inside the top and bottom walls since these boundaries are assumed to be heat insulated. It is found that the velocity profiles have the same trend and close values with $Ra = 10^8$ and $Ra = 10^9$. But then, the velocity

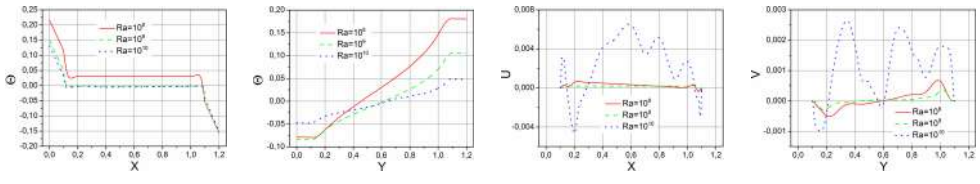

(a) (b) (c) (d)

Fig. 7. Temperature (a) and (b) and velocity (c) and (d) profiles when $a_{f,s} = 89.82$, $\lambda_{f,s} = 0.26$ and $Bi = 23$ in the sections of: (a), (c) $Y = 0.6$; (b), (d) $X = 0.6$.

curves become chaotic when the Rayleigh number is set to 10^{10} since a fully turbulent flow behavior is formed. Along with that, the absolute values of vector velocity components are drastically raised.

3.2. *The effect of $a_{f,s}$*

When considering the conjugate heat transfer formulation, the thermal properties of the enclosure are of great importance. Typical isotherms and streamlines with variation of $a_{f,s}$ and $\lambda_{f,s}$ are shown in Fig. 8.

Under the studied range of the governing parameters, the temperature of the fluid filling the cavity is increased with an increment in the heat diffusivity ratio and the thermal conductivity ratio. These patterns are obviously concerned with an enhancement in the thermal resistance of the enclosure. It is interesting to note that there is no clear thermal stratification in a range of the governing parameters under study. Relatively high-temperature gradients near the isothermal walls contribute to an active formation of convective plumes at the vertical solid–fluid interfaces. Thereby, many small turbulent eddies are created inside the main vortex. As a result, a complex flow pattern is observed in the solution domain. It is found that the isotherms configuration is almost the same inside the heated and cooled solid

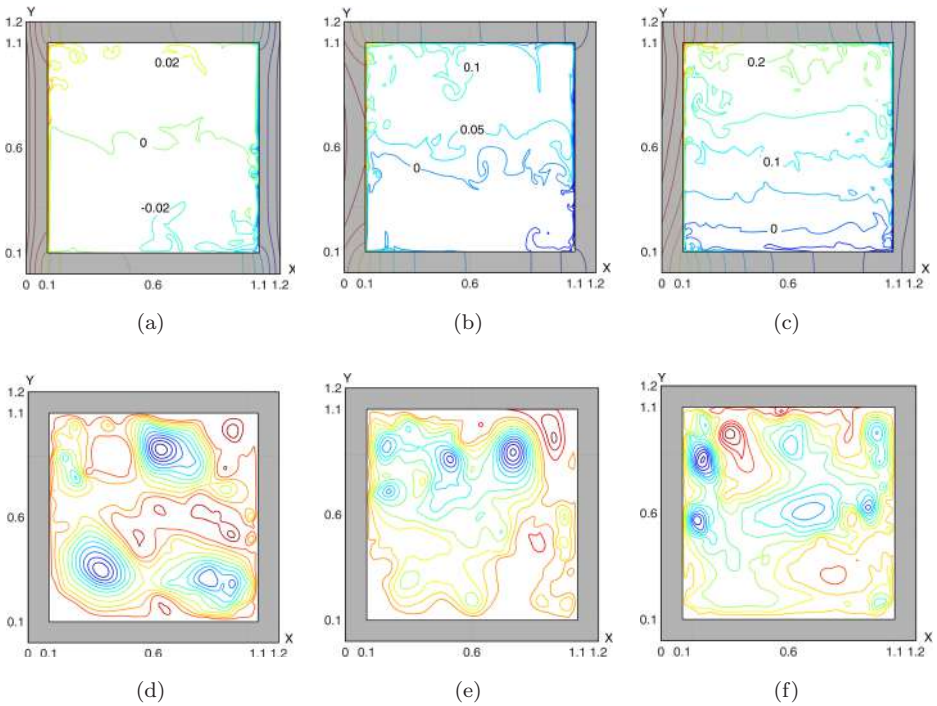

Fig. 8. Isotherms (a)–(c) and streamlines (d)–(f) when $Ra = 10^{10}$ and $Bi = 10$: (a), (d) $a_{f,s} = 1.67$, $\lambda_{f,s} = 0.00056$; (b), (e) $a_{f,s} = 7.67$, $\lambda_{f,s} = 0.0026$; (c), (f) $a_{f,s} = 26.42$, $\lambda_{f,s} = 0.0152$.

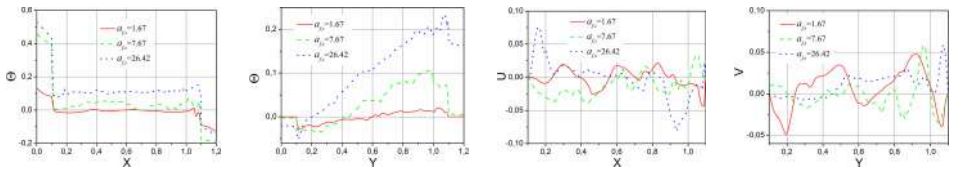

(a) (b) (c) (d)

Fig. 9. Temperature (a), (b) and velocity (c), (d) profiles when $Ra = 10^{10}$ and $Bi = 10$ in the sections of: (a), (c) $Y = 0.6$; (b), (d) $X = 0.6$.

vertical walls in a range of $1.67 \leq a_{f,s} \leq 7.67$ and $0.00056 \leq \lambda_{f,s} \leq 0.0026$. Moreover, the maximum value of the temperature is observed in the section of $Y = 0.6$ in this case whereas the temperature extremum is shifted to the top left corner when $a_{f,s} = 26.42$. It is revealed that cooling and heating rates are slightly different with $a_{f,s} = 1.67$ and $\lambda_{f,s} = 0.00056$. The thermal and flow behavior is approximately similar in terms of the thermal plumes, inner and outer currents locations in a range of $1.67 \leq a_{f,s} \leq 7.67$ and $0.00056 \leq \lambda_{f,s} \leq 0.0026$. On the other hand, the area of outer flows is shifted to the left top corner with $a_{f,s} = 26.42$ and $\lambda_{f,s} = 0.0152$. Along with that, the dimension of the main convective cell is increased. Probably, this regularity is due to an increment in the velocity of the upward and downward flows formed near the vertical solid–fluid interfaces. Variation of the local temperatures and velocities are given in Fig. 9.

According to the line graphs shown in Fig. 9, the temperature gradient inside the heated solid wall is raised as the thermal diffusivity ratio is increased. Along with that, a sharp drop of temperature is observed near the hot and cold solid–fluid interface. The temperature profiles are oscillatory due to the turbulent flow behavior. In general, an upward trend of the fluid temperature is noticed in the section of $X = 0.6$. This pattern is concerned with the natural convective mechanism of heat transfer. The air heated at the left solid–fluid interface is ascended along the Y-axis. It should be stressed that the temperature is slumped near the top solid–fluid interface since the energy is accumulated by a heat-conducting wall of finite thickness. However, the temperature gradient in this area is reduced with a decrease in the thermal conductivity ratio as could be predicted. When analyzing the velocity profiles, it is found that the maximum absolute values of U and V are grown as the heat diffusivity ratio is increased.

3.3. *Heat transfer rate*

The mean Nusselt numbers at the solid-fluid interfaces heated and cooled from the side are shown in Fig. 10.

When analyzing the heat transfer rate at the right wall, the mean Nusselt number is raised as the Biot number is grown. This pattern is predictable since the near-wall temperature gradient is increased with an increment in the thermal resistance to

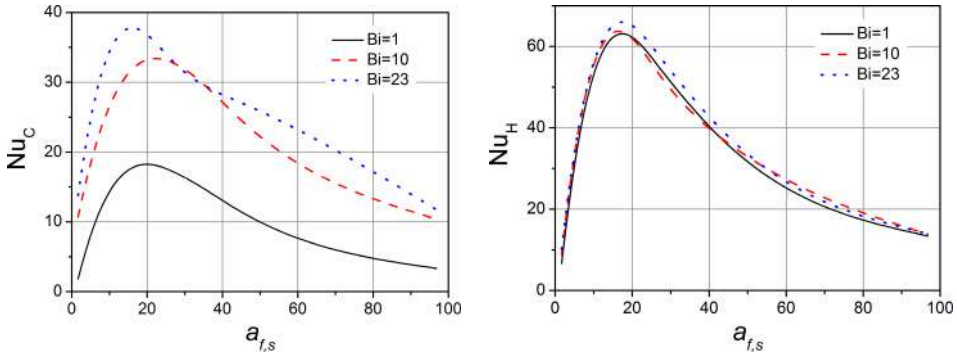

(a) (b)

Fig. 10. Temperature (a), (b) and velocity (c), (d) profiles when Nusselt number profiles when $Ra = 10^{10}$ at the: (a) left solid-fluid interface; (b) right solid-fluid interface.

conduction. At first glance, it would seem that an unexpected behavior is revealed when observing the $\mathrm{Nu} - a_{f,s}$ relation. The highest value of the Nusselt number is not achieved with the lowest thermal resistance of the enclosure. Probably, this regularity is concerned with the outside heating of the wall by constant heat flux. The low thermal conductivity of the enclosure prevents the heat transport into the cavity. Hence, the heat transfer rate is insignificant. When incrementing the heat diffusivity ratio, the thermal resistance of the walls is reduced and the temperature of the solution domain is grown. As a result, the mean Nusselt number at the right solid–fluid interface is increased. However, it should be stressed that a decrement in the thermal resistance is followed by the enhancement of the heat losses through the right wall. Therefore, the Nusselt number goes up reaching the peak, and then the Nu steadily declines. When varying the heat-diffusivity ratio, the Bi determines both the heat transfer rate and the location of the function extremum. However, despite the different values of the Nu_C, the curves show the same pattern for different values of the Biot numbers. On the contrary, the variation of the Bi slightly affects the heat transfer rate at the left solid-fluid interface heated from the outside.

4. Conclusion

A relatively simple and robust approach is proposed to study the effect of conduction in the walls on the turbulent buoyancy-driven flow. The proposed hybrid model imitates pseudo-DNS technique and contains no empirical input data as the RANS does. Hence, it can be considered as a universal tool for simulation for both forced and natural convection. When performing the simulations, the following specific patterns are revealed:

- When taking into account the thermal conduction in the enclosure, the heat transfer rate is weakened due to the energy accumulation by the solid walls of

finite thickness. The Rayleigh number variation slightly affects the temperature of the right wall whereas the temperature of the heat-insulated walls is changed. The heat-conductivity of the enclosure determines the magnitude of the temperature gradient inside the left and right walls.

- Variation of the heat diffusivity ratio significantly affects the thermal and flow behavior. The convective plumes are formed both at the vertical and horizontal solid-fluid interfaces. The gradient of temperature inside the left wall is increased with an increment in the thermal diffusivity ratio. The temperature sharply declines near the hot and cold interfaces.
- Fluid is a radiatively non-participating medium. The Biot number specifies the extremum of the $\mathrm{Nu}_C - a_{f,s}$ curves and the heat transfer rate at the right solid-fluid interface. On the other hand, the mean Nusselt number at the left interface is slightly varied with the *Bi*.

Acknowledgments

The research was carried out within the framework of Tomsk Polytechnic University Development Program.

References

Ben-Nakhi, A. and Mahmoud, M. A. [2008] "Conjugate turbulent natural convection in the roof enclosure of a heavy construction building during winter," *Applied Thermal Engineering* **28**, 1522–1535.

Ben Yedder, R. and Bilgen, E. [1997] "Laminar natural convection in inclined enclosures bounded by a solid wall," *Heat and Mass Transfer* **32**, 455–462.

Ben Yedder, R. and Bilgen, E. [1999] "Turbulent natural convection in a square enclosure bounded by a solid wall with localized heating," *Heat and Mass Transfer* **35**, 401–408.

Bettaibi, S., Kuznik, F. and Sediki, E. [2016] "Hybrid LBM-MRT model coupled with finite difference method for double-diffusive mixed convection in rectangular enclosure with insulated moving lid," *Physica A* **444**, 311–326.

Dixit, H. N. and Babu, V. [2006] "Simulation of high Rayleigh number natural convection in a square cavity using the lattice Boltzmann method," *International Journal of Heat and Mass Transfer* **49**, 727–739.

Ginzburg, I., Verhaeghe, F. and d'Humieres, D. [2008] "Study of simple hydrodynamic solutions with the two-relaxation-times lattice Boltzmann scheme," *Communications in Computational Physics* **3**, 519–581.

Kuznetsov, G. V. and Sheremet, M. A. [2010] "Numerical simulation of turbulent natural convection in a rectangular enclosure having finite thickness walls," *International Journal of Heat and Mass Transfer* **53**, 163–177.

Kuznetsov, G. V., Kurinlenko, N. I. and Nee, A. E. [2018] "Mathematical modelling of conjugate heat transfer and fluid flow inside a domain with a radiant heating system," *International Journal of Thermal Sciences* **131**, 27–39.

Lallemand, P. and Lou, L.-S. [2003] "Hybrid finite-difference thermal lattice Boltzmann equation," *International Journal of Modern Physics B* **17**, 41–47.

Mikhailenko, S. A., Miroshnichenko, I. V. and Sheremet, M. A. [2021] "Thermal radiation and natural convection in a large-scale enclosure heated from below: Building application," *Building Simulation* **14**, 681–691.

Miroshnichenko, I. V., Sheremet, M. A. and Mohamad, A. A. [2016] "Numerical simulation of a conjugate turbulent natural convection combined with surface thermal radiation in an enclosure with a heat source," *International Journal of Thermal Sciences* **109**, 172–181.

Miroshnichenko, I. V. and Sheremet, M. A. [2018] "Radiation effect on conjugate turbulent natural convection in a cavity with a discrete heater," *Applied Mathematics and Computation* **321**, 358–371.

Nee, A. [2020] "Hybrid meso-macroscopic simulation of three-dimensional natural convection combined with conjugate heat transfer," *Thermal Science and Engineering Progress* **19**, 100584.

Obrecht, Ch., Kuznik, F., Tourancheau, B. and Roux, J.-J. [2013] "Multi-GPU implementation of a hybrid thermal lattice Boltzmann solver using the TheLMA framework," *Computers & Fluids* **80**, 269–275.

Olazo-Gomez, Y., Xaman, J., Gijon-Rivera, M., Noh-Pat, F., Sima, E. and Chavez, Y. [2020] "Mathematical modelling of conjugate laminar and turbulent heat transfer in a cavity: Effect of a vertical glazed wall," *International Journal of Thermal Sciences* **152**, 106310.

Rahimi, A., Azarikhah, P., Kasaeipoor, A., Malekshah, E. H. and Kolsi., K. [2019] "Lattice Boltzmann simulation of free convection's hydrothermal aspects in a finned/multi-pipe cavity filled with CuO–water nanofluid," *International Journal of Numerical Methods for Heat & Fluid Flow* **29**, 1058–1078.

Rahimi, A., Kasaeipoor, A., Amiri., A., Doranehgard., M. H., Malekshah, E. H. and Kolsi., K. [2018] "Lattice Boltzmann method based on Dual-MRT model for three-dimensional natural convection and entropy generation in CuO–water nanofluid filled cuboid enclosure included with discrete active walls," *Computers & Mathematics with Applications* **75**, 1795–1813.

Sharma, A. K., Velusamy, K. and Balaji, C. [2008] "Conjugate transient natural convection in a cylindrical enclosure with internal volumetric heat generation," *Annals of Nuclear Energy* **35**, 1502–1514.

Sharma, K. V., Straka, R. and Tavares, F. W. [2018] "Natural convection heat transfer modeling by the cascaded thermal lattice Boltzmann method," *International Journal of Thermal Sciences* **134**, 552–564.

Sergent, A., Xin, Sh., Joubert, P., Le Quéré, P., Salat, J. and Penot, F. [2013a] "Resolving the stratification discrepancy of turbulent natural convection in differentially heated air-filled cavities – Part I: Reference solutions using Chebyshev spectral methods," *International Journal of Heat and Fluid Flow* **39**, 1–14.

Sergent, A., Joubert, P., Xin, Sh. and Le Quéré, P. [2013b] "Resolving the stratification discrepancy of turbulent natural convection in differentially heated air-filled cavities Part II: End walls effects using large eddy simulation," *International Journal of Heat and Fluid Flow* **39**, 15–27.

Sheremet, M. A. and Miroshnichenko, I. V. [2015] "Numerical study of turbulent natural convection in a cube having finite thickness heat-conducting walls," *Heat and Mass Transfer* **51**, 1559–1569.

Wang, P., Zhang, Yo. and Gou, Zh. [2017] "Numerical study of three-dimensional natural convection in a cubical cavity at high Rayleigh numbers," *International Journal of Heat and Mass Transfer* **113**, 217–228.

Xaman, J., Arce, J., Alvarez, G. and Chavez, Y. [2008] "Laminar and turbulent natural convection combined with surface thermal radiation in a square cavity with a glass wall," *International Journal of Thermal Sciences* **47**, 1630–1638.

Xaman, J., Alvarez, G., Hinojosa, J. and Flores, J. [2009] "Conjugate turbulent heat transfer in a square cavity with a solar control coating deposited to a vertical semi-transparent wall," *International Journal of Heat and Fluid Flow* **30**, 237–248.

Xin, Sh., Salat, J., Joubert, P., Sergent, A., Penot, F. and Le Quéré, P. [2013] "Resolving the stratification discrepancy of turbulent natural convection in differentially heated air-filled cavities. Part III: A full convection–conduction–surface radiation coupling," *International Journal of Heat and Fluid Flow* **39**, 33–48.

Xin, Sh. and Le Quéré, P. [1994] *Direct and Large-Eddy Simulation I. Fluid Mechanics and Its Applications* (Springer, Dordrecht).

Zhuo, C. and Zhong, Ch. [2013] "LES-based filter-matrix lattice Boltzmann model for simulating turbulent natural convection in a square cavity," *International Journal of Heat and Fluid Flow* **42**, 10–22.